BB

SERVICE DE PHYSIQUE NUCLÉAIRE

CEA
C.E. SACLAY
DSM
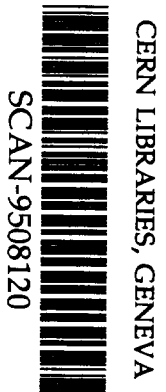
SW9533
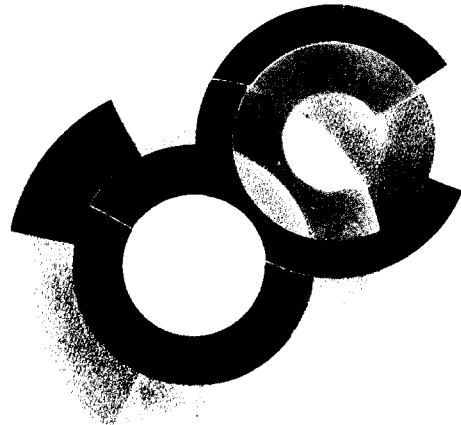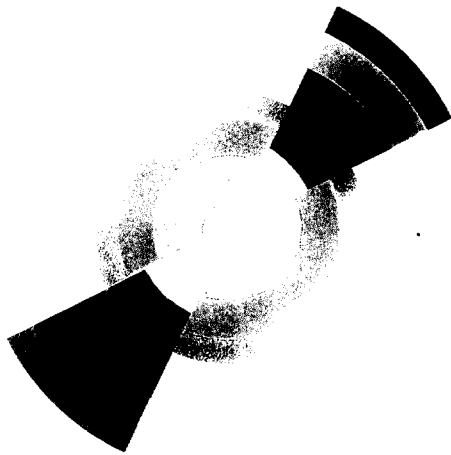
DAPNIA

DAPNIA/SPhN 95 07   03/1995

EVOLUTION OF REACTION MECHANISMS FOR THE

REACTION ^{36}Ar+^{58}Ni STUDIED FROM 32 to 95 A·MeV

WITH THE INDRA MULTIDETECTOR*

E. De Filippo[3], G. Auger[1], Ch.O. Bacri[2], A. Benkirane[1], J. Benlliure[1], B. Berthier[3],
B. Borderie[2], R. Bougault[4], P. Box[2], R. Brou[4], Y. Cassagnou[3], J-L. Charvet[3],
A. Chbihi[1], J. Colin[4], D. Cussol[4], R. Dayras[3], A. Demeyer[5], D. Durand[4],
P. Ecomard[1], P. Eudes[6], A. Genoux-Lubain[4], D. Gourio[6], D. Guinet[5],
L. Lakehal-Ayat[2], P. Lautesse[5], P. Lautridou[6], J.L. Laville[6], L. Lebreton[5],
C. Le Brun[4], J.F. Lecolley[4], A. Lefevre[1], R. Legrain[3], O. Lopez[4], M. Louvel[4],
N. Marie[1], V. Métivier[4], L. Nalpas[3], T. Nakagawa[4], A. Ouatizerga[2], M. Parlog[2],
J. Péter[4], E. Plagnol[2], E.C. Pollacco[3], J. Pouthas[1], A. Rahmani[6], R. Regimbart[4],
M.F. Rivet[2], T. Reposeur[6], E. Rosato[4], F. Saint-Laurent[1], M. Squalli[2],
J.C. Steckmeyer[4], B. Tamain[4], L. Tassan-Got[2], E. Vient[4], C. Volant[3],
J.P. Wieleczko[1], A. Wieloch[4] and K. Yuasa-Nakagawa[4].

EVOLUTION OF REACTION MECHANISMS FOR THE REACTION ^{36}Ar+^{58}Ni STUDIED FROM 32 to 95 A·MeV WITH THE INDRA MULTIDETECTOR[*]

E. De Filippo[3], G. Auger[1], Ch.O. Bacri[2], A. Benkirane[1], J. Benlliure[1], B. Berthier[3],
B. Borderie[2], R. Bougault[4], P. Box[2], R. Brou[4], Y. Cassagnou[3], J-L. Charvet[3],
A. Chbihi[1], J. Colin[4], D. Cussol[4], R. Dayras[3], A. Demeyer[5], D. Durand[4],
P. Ecomard[1], P. Eudes[6], A. Genoux-Lubain[4], D. Gourio[6], D. Guinet[5],
L. Lakehal-Ayat[2], P. Lautesse[5], P. Lautridou[6], J.L. Laville[6], L. Lebreton[5],
C. Le Brun[4], J.F. Lecolley[4], A. Le Fèvre[1], R. Legrain[3], O. Lopez[4], M. Louvel[4],
N. Marie[1], V. Métivier[4], L. Nalpas[3], T. Nakagawa[4], A. Ouatizerga[2], M. Parlog[2],
J. Péter[4], E. Plagnol[2], E.C. Pollacco[3], J. Pouthas[1], A. Rahmani[6], R. Regimbart[4],
M.F. Rivet[2], T. Reposeur[6], E. Rosato[4], F. Saint-Laurent[1], M. Squalli[2],
J.C. Steckmeyer[4], B. Tamain[4], L. Tassan-Got[2], E. Vient[4], C. Volant[3],
J.P. Wieleczko[1], A. Wieloch[4] and K. Yuasa-Nakagawa[4].

(1) GANIL, B.P.5027 - 14021 Caen Cedex, France
(2) IPN, IN2P3-Université Paris Sud, F-91406 Orsay, France
(3) CEA, DAPNIA/SPhN, CE Saclay, F-91191 Gif-sur-Yvette Cedex, France
(4) LPC, ISMRA, IN2P3-CNRS F-14050 Caen Cedex, France
(5) IPN Lyon, IN2P3-CNRS et Université, F-69622 Villeurbanne Cedex, France
(6) SUBATECH, IN2P3-CNRS et Université, F-44072 Nantes Cedex 03, France

Abstract

In the context of the multifragmentation study program with the 4π INDRA detector at GANIL, the reaction ^{36}Ar+^{58}Ni has been studied at seven different energies ranging from 32 to 95 A·MeV. After a brief description of the detector characteristics and of the data treatment, results on the evolution of IMF distributions with incident energy and a first outlook about reaction mechanisms will be presented.

---

[*]Experiment performed at GANIL

Talk presented to the XXXIII Winter Meeting on Nuclear Physics, Bormio (Italy)

I. INTRODUCTION

Nuclear multifragmentation has been experimentally observed [1], but total understanding of this phenomenon has not yet been reached. While at low excitation energy nuclei decay essentially by emitting neutrons and light charged particles, as the excitation energy increases emission of intermediate mass fragments (IMF) occurs. Whether this multifragment emission can be described in terms of a statistical evaporation process, or as a process in which fragments are emitted almost simultaneously (the so called "true" multifragmentation) is still an open question. Dynamical calculations predict, for central collisions, the occurrence of a compression phase [2,3] followed by an expansion phase during which the system, due to growth of density fluctuations, can disassemble in many fragments. Whether this process is accompanied or not by a liquid-phase transition is another debated question. To explore those aspects of the multifragmentation process the INDRA multidetector has been used, starting from 1993, to study a large variety of systems as a function of various parameters as incident energy, size of the system, mass asymmetry, etc. The reaction Ar+Ni, which is the object of this talk, together with the Ni+Ni system, is part of a general study whose one of the goal is the measurement of nuclear flow [4–6] that yields information about the incompressibility modulus K_∞ and the nucleon-nucleon cross section in nuclear matter.

The experimental set-up will be presented in section 2 together with a description of event selection criteria. In section 3 will be shown results concerning IMF distributions and their evolution with incident energy. In section 4 qualitative results about reaction mechanisms will be presented for some particular classes of events. In section 5 a discussion about impact parameter determination is reported.

II. EXPERIMENTAL SET-UP

The Ar+Ni experiment was performed at GANIL with the 4π INDRA detector, a detailed description of which, together with description of charge identification and calibration procedures, can be found in Ref. [7]. Very briefly INDRA is made of 336 telescopes with a geometric efficiency of 90% of the 4π solid angle, distributed over 17 rings centered around the beam axis. The first ring (2°-3°) which may sustain a high flux of elastically scattered particles is made of 12 fast counting phoswich scintillators (0.5mm thick NE102 plastic followed by a 25 cm long NE115 plastic). From 3° to 45°, due to the required large energy dynamic range, rings 2 to 9 are constituted by 180 three-stage telescopes made of an axial field 5cm deep ionization chamber operated at 50mb of C_3F_8 gas, a 300μm thick silicon detector and a CsI crystal scintillator

thick enough to stop all particles. The angular range from 45° to 176° is covered by rings 10 to 17 made of 144 two-stage telescopes each consisting of an axial field ionization chamber operated at 30mb and a CsI crystal scintillator. For calibration purposes, one module of each ring from 10 to 17 contains a telescope (80μm Si + 2mm Si(Li)) between the ionization chamber and the CsI crystal. The ionization chambers insure an energy threshold for fragments of $\approx$ 1 A·MeV. For particles with charge Z$\leq$4, isotopic separation can be achieved in the CsI detectors using pulse shape discrimination techniques. Energy calibrations of all detector modules were performed using α sources, elastically scattered low energy heavy ions and secondary light charged particle beams.

In the experiment a ^{58}Ni target, 193 μg/cm^2 thick, was bombarded with an ^{36}Ar beam at incident energies of 32,40,52,63,74,84 and 95 A·MeV. All lower energies were obtained by slowing down the original 95 A·MeV beam. Beam intensity was kept around 10^7 particles/s in order to maintain multiple interaction probability in the target below 10^{-6}. A trigger based on multiplicity was used. Only events for which multiplicity was greater or equal to 3 (4 for incident energies of 84 and 95 A·MeV) were registered. In these conditions the dead time of the acquisition system was maintained below 20%. For this experiment the backward ionization chambers at angles greater than 90° were not installed.

A. Event selection criteria

In Fig. 1, the total detected charge (Z_{tot}) of identified particles is reported as a function of the total charged particles multiplicity at incident beam energies of 32, 52 and 95 A·MeV. These correlations are very representative of the INDRA detector efficiency. Every plot can be easily divided in three regions: at low multiplicity, two regions, one where Z_{tot} is lower than 10 and the other at $Z_{tot}\approx$18 can be easily distinguished. These low multiplicity regions are associated with peripheral reactions, generally characterized by the presence of two fragments, a project-like fragment (PLF), emitted at forward angles with a velocity close to the projectile velocity and a massive low energy partner (target-like fragment or TLF). In the zone of lowest Z_{tot} both the PLF and TLF are not detected, in the second zone ($Z_{tot}\approx$18) the PLF is detected but the TLF, because of its low velocity, is below the detection threshold. For all energies there is a well delineated region of events where a large fraction of the total charge is detected. We have considered in our analysis only events for which the total detected charge is greater than 38, corresponding to over 80% of the system total charge which is Z=46. The selection made is represented by the horizontal line in fig. 1. The main effect of this selection is to reject the more peripheral collisions

3

or badly detected events. In Fig. 2, the evolution of the charged product multiplicity is followed as a function of the bombarding energy. While at low energies two bumps are clearly visible corresponding to peripheral (low multiplicity) and more central collisions (high multiplicity), at increasing energy the high multiplicity bump is less pronounced whereas the maximum multiplicity increases. It is interesting to note that at 95 A·MeV the maximum multiplicity reaches values close to the total charge of the system. As a rough estimate of the impact parameter a calculation has been made assuming a monotonic relationship between multiplicity and impact parameter [8]. Before to do so, it has been checked that the measured reaction cross-sections which decrease from about 3b at 32 A·MeV to 2.8b at 95 A·MeV agree within 10% with the systematics of Kox et al. [9]. The impact parameter scale is indicated for some energies in Fig. 2. When a selection upon the total charge is made ($Z_{tot} \geq 38$) the corresponding multiplicity distribution is bell shaped and extend from a value of $\sim$10 to the highest multiplicity value.

III. IMF DISTRIBUTIONS

We shall define as IMF (intermediate mass fragments) all fragments with charge greater than or equal to 3 and we shall consider only almost complete events as defined in the preceding section. Fig. 3a displays the evolution of IMF distributions at 3 different bombarding energies 32, 52 and 95 A·MeV. Distributions are normalized to their respective areas. The partition of the system in IMF is dominated by events with 2 and 3 IMF and the shape as well as the mean values of the distributions do not seem to depend on the bombarding energy. This can be seen in Fig. 3b where the relative proportion of events containing a given number of IMF is plotted as a function of the incident energy from 32 to 95 A·MeV. Only events with no-IMF show a dependence on incident energy: the relative proportion of these events sharply raises starting from about 40 A·MeV bombarding energy. These events without IMF are slightly different from those called vaporization events (break-up into H and He isotopes only) elsewhere [10]; the latter were selected by taking account efficiency effects and their onset was found around 50 A·MeV. However the average size <Z> of the fragments strongly diminishes as the incident energy increases. For instance, for events with 1 detected IMF, the average charge of the fragment is 21 at 32 A·MeV and 7 at 95 A·MeV; for events with 2 detected IMF the average charge decreases from 12 at 32 A·MeV to 6 at 95 A·MeV. At the same incident energy the average size of the IMFs decreases as the number of IMFs increases. This latter effect is due essentially to charge conservation. Finally in Fig. 4 the average total charged particle multiplicity is plotted as a function of the number of IMFs in a given event. While

4

at incident energies 32 and 40 A·MeV the average multiplicity stays almost constant with the number of IMFs, at higher bombarding energies the average multiplicity increases when the number of IMFs per event decreases, the maximum in multiplicity being reached for no-IMFs events.

IV. EVOLUTION OF REACTION MECHANISMS

We want now to study some qualitative aspects of the evolution of the reaction mechanisms for the reaction Ar+Ni. We shall present some results regarding two particular classes of events: complete events in which 1 IMF or 2 IMFs have been detected. Charged particle multiplicity was used as a rough estimate of the centrality of the collision, as illustrated in Fig. 5 for 1 IMF events. By dividing the total multiplicity distributions for these events in two parts, the highest half of the multiplicity distribution is associated to the most violent collisions. As we can see in the figure, the lowest part of the multiplicity distribution is still associated to relatively low values of the reduced impact parameter, the most peripheral collisions have been rejected.

Complete events containing 1 IMF have been selected at 32 and 95 A·MeV. A suggestion about the mechanism of the collision is given by the number of sources. Complete fusion is characterized by one source with the velocity of the center of mass. If the reaction is essentially binary, two sources (a fast one and a slow one) of reaction products should be observed. The Lorentz invariant cross-section $d^2\sigma/\beta_\perp d\beta_\perp d\beta_\parallel$ has been plotted in Fig. 6, for Z=2 particles at 32 A·MeV incident energy. Fig. 6a refers to the low multiplicy slice and Fig. 6b to the high multiplicity one (M≥16). In both cases source separation is hardly seen, but there is evidence of a source centered below the center of mass velocity. However, when high multiplicities are selected, the presence of Z=2 particles coming from a fast source could be an indication of pre-equilibrium particle emission. If we look at the corresponding IMF laboratory velocity distribution (Fig. 7a) it is peaked well below the center of mass velocity at about 2 cm/ns, near the detection threshold. This picture is compatible with a process in which the observed IMF is the evaporation residue of an incomplete fusion process (with about 60% momentum transfer). The fact that the IMF angular distribution is, at 32 A·MeV, strongly forward peaked seems to confirm this hypothesis. A clear evolution in the reaction mechanisms is observed when going to 95 A·MeV bombarding energy. The Lorentz invariant cross-section for Z=2 particles at this incident energy (Fig. 6cd) shows essentially two sources. A fast one whose velocity is near the projectile velocity and a slow one centered around the target velocity. The corresponding IMF velocity distribution (Fig. 7b) is broad and extends from detection threshold to a velocity corresponding to the projectile one. The distribution becomes shallower when the

5

highest multiplicity gate is imposed. Therefore the observed IMF could be considered as the remnant of a binary reaction where one of the two partners has completely disassembled in light charged particles.

The appearing of a binary process for 1 IMF events and central collision at 95 A·MeV is very intriguing. Results of a Landau-Vlasov calculation [11] are shown in Fig. 8. The calculation has been done at 0.5 fm impact parameter using Gogny D1-G1 force. Density profiles for the reaction Ar+Ni at 95 A·MeV are plotted at time steps of 10 fm/c from 0 to 160 fm/c. The calculation predict for very central collisions a final binary system that is formed due to a transparency effect.

Complete events with 2 IMFs have been analyzed in the aim to better characterize the relative contribution of mechanisms like fusion or deep inelastic processes. As before total multiplicity distribution for these events has been divided in two parts to select the centrality of the collision. In Fig. 9a and Fig.9b the relative velocity between the two IMFs is reported as a function of their parallel velocities respectively for the low multiplity gate and the high multiplicity gate at the energy of 32 A·MeV. Two branches associated with a fast fragment (parallel velocity near the projectile velocity) and a slow partner (parallel velocity below center of mass velocity) are clearly seen. They are products of a binary deep inelastic type reaction. This process remains dominant also when a high multiplicity gate is imposed, but in this case the fraction of more damped reactions (small relative velocity) or completely damped reactions grows. The binary character of the reaction is confirmed when the relative velocity between the two fragments is reported as a function of the angle θ between the relative velocity and the beam direction (Fig. 9cd). Here a strong correlation between relative velocity and emission angle can be seen as in a classical deep inelastic collision. The same analysis at 95 A·MeV bombarding energy gives similar results but, in this case, the relative velocity remains well above the velocity corresponding to the Coulomb repulsion between fragments ($\sim$ 2.5 cm/ns), i.e. completely damping is almost never reached even when we select the most central collisions. As already observed in the study of nearly symmetrical systems (^{36}Ar + ^{27}Al and ^{64}Zn + ^{nat}Ti) [12] at energies greater than 35 A·MeV binary collision seems to be the dominant process even for the most central collisions.

V. SELECTION OF CENTRAL COLLISIONS

Total charged particle multiplicity has been used to classify roughly the events according to the impact parameter. However the experimental determination of the impact parameter may depend upon the global variable (or combination of global variables) that has been used [13]. The relation between the total charged particle

6

multiplicity and the impact parameter has been tested through simulations incorporating the detector filter. The link between the total transverse kinetic energy [14] and the impact parameter has also been verified. The transverse energy is defined as $E_t = \sum_i E_i \sin^2 \theta_i$ where E_i is the kinetic energy and θ_i the emission polar angle of the particle i with respect to the beam axis. The total transverse kinetic energy is reported in Fig. 10a as a function of the total charged particle multiplicity at the bombarding energy of 95 A·MeV. The two variables are strongly correlated but the multiplicity tends to saturate at high values of E_t as already noticed in Ref. [13]. The simulation was performed with an event generator code described in Ref. [15]. Simulated data were filtered to take into account the INDRA geometry. In Fig. 10b the simulated total charged multiplicity vs. E_t is reported for comparison with the experimental data of Fig. 10a. The two maps are very similar. Therefore the average total multiplicity (Fig. 10c) and the average E_t (Fig. 10d) has been calculated in a event by event analysis with the simulated data as a function of the impact parameter. It is clear in Fig. 10c that total charged particle multiplicity saturates at low impact parameters, and thus the total multiplicity is a bad indicator of the impact parameter below about 4 fm. On the contrary the E_t vs impact parameter plot presents a greater linearity at low values of impact parameter. These results show that when a good sensitivity to impact parameter variations for central collision is requested great care has to be taken in using the total charged particle multiplicity. In these cases, more sophisticated techniques or combination of different global variables have to be used.

VI. CONCLUSION

The evolution of the reaction mechanism in the Ar + Ni system has been studied with the INDRA multidetector over a wide range of energies from 32 to 95 A·MeV. Global features of this reaction were presented regarding particularly IMF distributions and multiplicities. Complete events with 1 IMF or 2 IMFs were selected in the aim to obtain some qualitative information about reaction mechanisms. Total multiplicity was used in a first simple approximation to select more central collisions. When 1 IMF events are selected, for central collisions, at 32 A·MeV results seem compatible with a process where the IMF could be the evaporation residue of an incomplete fusion process; more complex mechanisms occurs at 95 A·MeV. At this energy Landau-Vlasov calculations predicts transparency effects in central collisions. Study of 2 IMF events shows that binary collision dynamics dominate also for more central collisions. The following of this analysis in a more quantitative way will require a better definition of the degree of centrality (or violence) of the collision: therefore the search for better central collision indicator than multiplicity is necessary.

REFERENCES

[1] L.G. Moretto and G.J. Wozniak, Ann. Rev. Nucl. Part. Sci. 43 (1993) 379 and references therein.

[2] J. Cugnon, Phys. Lett. B135 (1984) 374.

[3] E. Suraud, D. Cussol, Ch. Grégoire, D. Boiley, M. Pi, P. Schuck, B. Rémaud, and F. Sébille, Nucl. Phys. A495 (1989) 73c; E. Suraud, M. Pi, P. Schuck, B. Rémaud, F. Sébille, Ch. Grégoire and F. Saint-Laurent, Phys. Lett. B229 (1989) 359.

[4] V. de la Mota, F. Sébille, M. Farine, B. Rémaud and P. Schuck, Phys. Rev. C46 (1992) 677.

[5] W.Q. Shen et al., Nucl. Phys. A551 (1993) 333.

[6] J.C. Angelique et al., preprint LPCC 94-10 (1994).

[7] J. Pouthas et al., accepted for publication in Nucl. Inst. and Meth. Preprint GANIL 94 26.

[8] C. Cavata et al., Phys. Rev. C42 (1990) 1760.

[9] S. Kox et al., Nucl. Phys. A420 (1984) 162.

[10] Ch.O. Bacri et al. submitted to Phys. Lett. B and to be published in Proceedings of the CORINNE II Int. Workshop on Multi-Particle Correlations and Nuclear Reactions (Nantes, France 1994) Word Scientific.

[11] V. de la Mota et al., Phys. Rev. C46 (1992) 677.

[12] A. Kerambrun et. al., Preprint LPCC 94-14 (1994).

[13] L. Phair et. al., Nucl. Phys. A548 (1992) 489.

[14] M.B. Tsang et al. Phys. Rev. C44 (1991) 2065.

[15] D. Durand, Nucl. Phys. A541 (1992) 266.

FIGURES

FIG. 1. Total detected charge as a function of total charged particle multiplicity at 32, 52 and 95 A·MeV bombarding energies for the Ar+Ni reaction. The horizontal line at Z_{tot}=38 indicates the lower limit choosen for the total charge to select almost complete events.

FIG. 2. Evolution of the total charged particle multiplicity distribution with the bombarding energy. Dashed curves are the multiplicity distributions when the condition $Z_{tot} \geq 38$ is imposed. For some energies an impact parameter scale is indicated on the top (see text).

FIG. 3. (a) IMF multiplicity distributions ($Z_{tot} \geq 38$) at 32,52 and 95 A·MeV bombarding energies and (b) Relative fraction of events ($Z_{tot} \geq 38$) with 0,1,2...6 IMFs as a function of bombarding energy.

FIG. 4. The average total charged particle multiplicity as a function the number of IMFs in a given event for the different bombarding energies from 32 to 95 A·MeV ($Z_{tot} \geq 38$).

FIG. 5. Total charged products multiplicity for complete events ($Z_{tot} \geq 38$) with only 1 IMF detected. The vertical line gives the selection on multiplicity made at various incident energies. The upper scale gives an estimate of the reduced impact parameter ($b_o \approx 10$ fm) (see text).

FIG. 6. Invariant cross-sections in the $\beta_\parallel$-$\beta_\perp$ plane for Z=2 particles ($Z_{tot} \geq 38$) at a), b) 32 A·MeV and c),d) 95 A·MeV. Arrows indicate center of mass and projectile velocities. Plots a) and c) are for low multiplicity selection b) and d) for high multiplicity selection.

FIG. 7. IMF velocity (cm/nsec) for 1 IMF complete events ($Z_{tot} \geq 38$) at a) 32 A·MeV and b) 95 A·MeV for the low and high multiplicity slices.

FIG. 8. Density profiles in a Landau-Vlasov calculation for the Ar+Ni reaction at 95 A·MeV and impact parameter b=0.5 fm. The time ranges from 0 to 160 fm/c in 10 fm/c steps scanning from left to right and from bottom to top.

9

FIG. 9. a), b) Relative fragment velocity as a function of their parallel velocity for 2 IMF events and c), d) Relative velocity as a function of angle between relative velocity and beam axis. Plots a) and c) are for low multiplicity selection b) and d) for high multiplicity selection.

FIG. 10. a) Experimental and b) simulated, total transversal kinetic energy E_t vs total charged particle multiplicity M. Simulated c) average M and d) average E_t as a function of the impact parameter (fm).

Fig. 1

^{36}Ar + ^{58}Ni

MULTIPLICITY

Fig. 2

Fig. 3

Ar + Ni

95 MeV/A
84 MeV/A
74 MeV/A
52 MeV/A
40 MeV/A
32 MeV/A

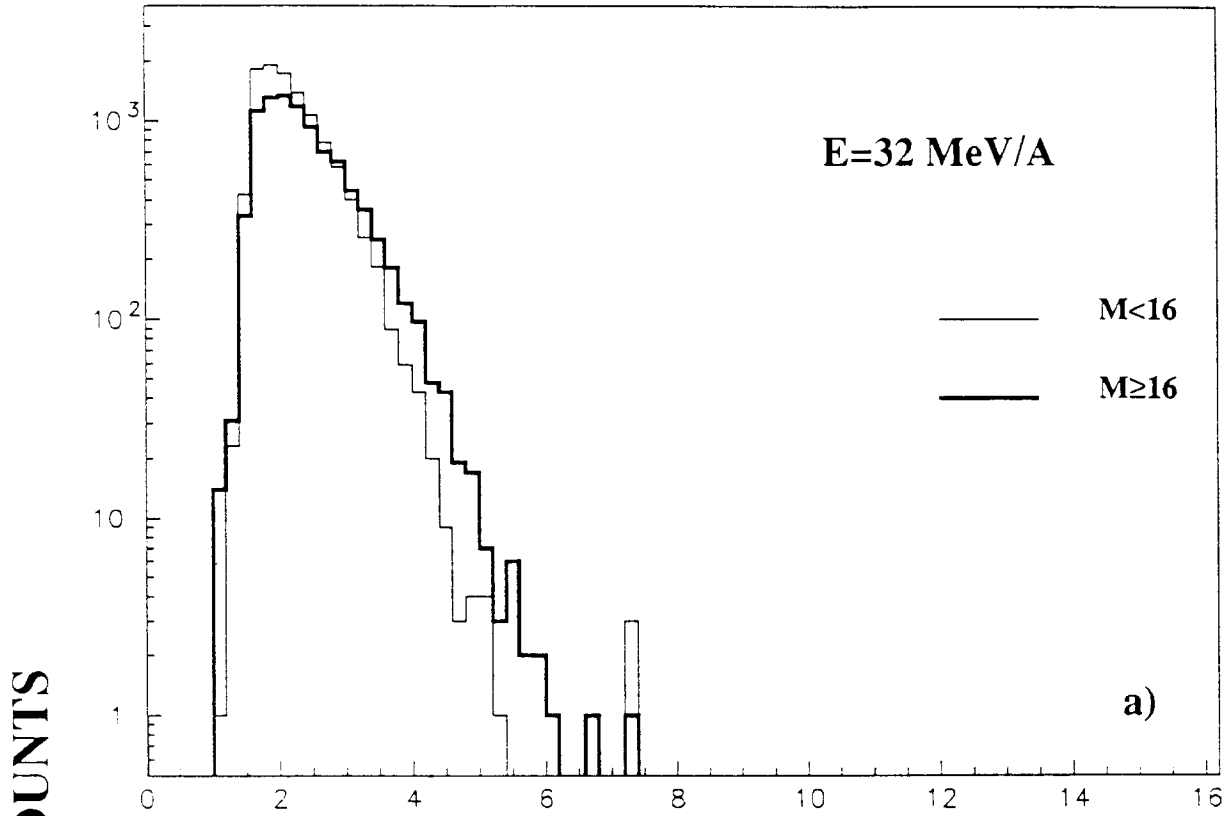〈TOTAL MULTIPLICITY〉
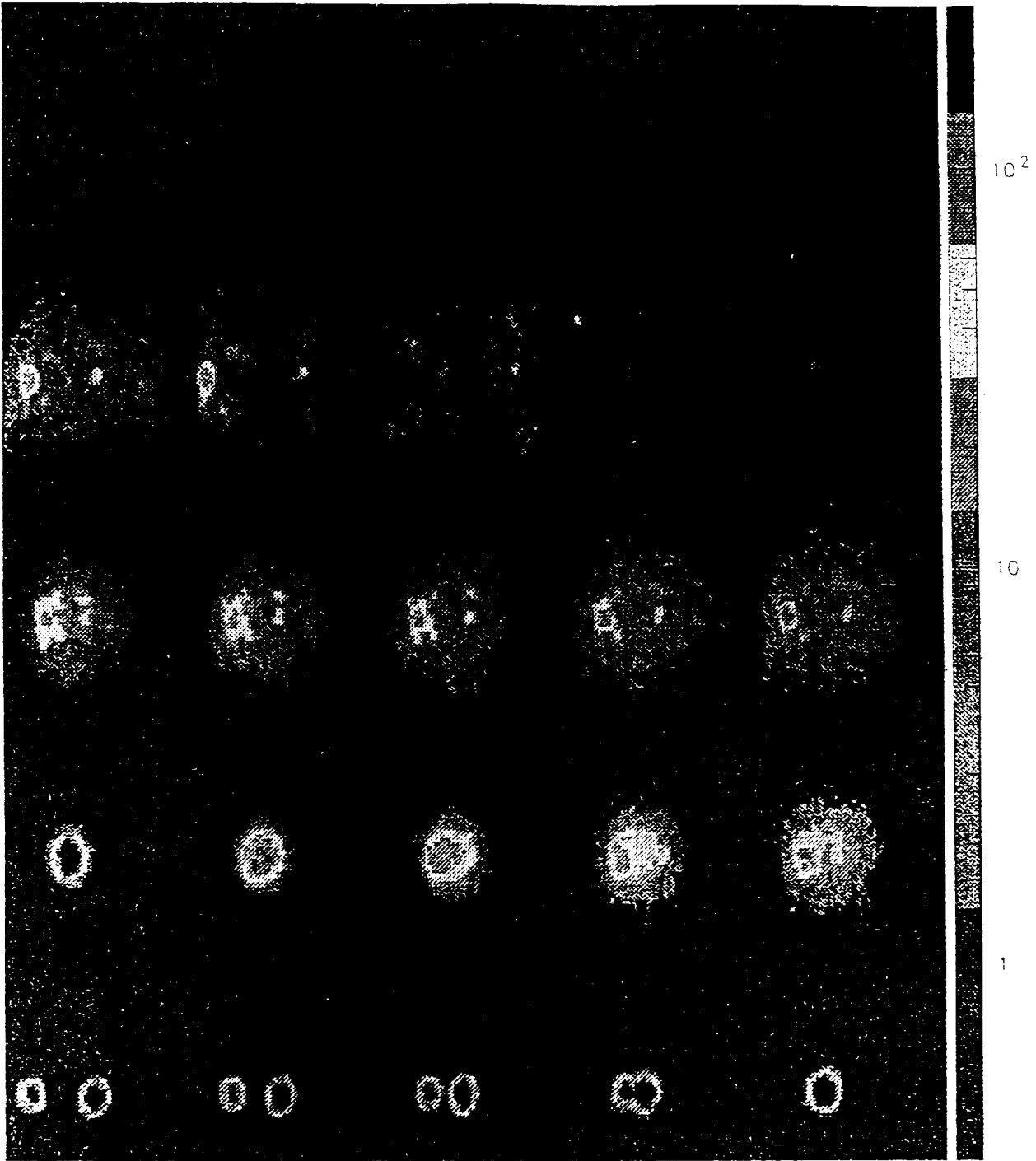
Number of IMF
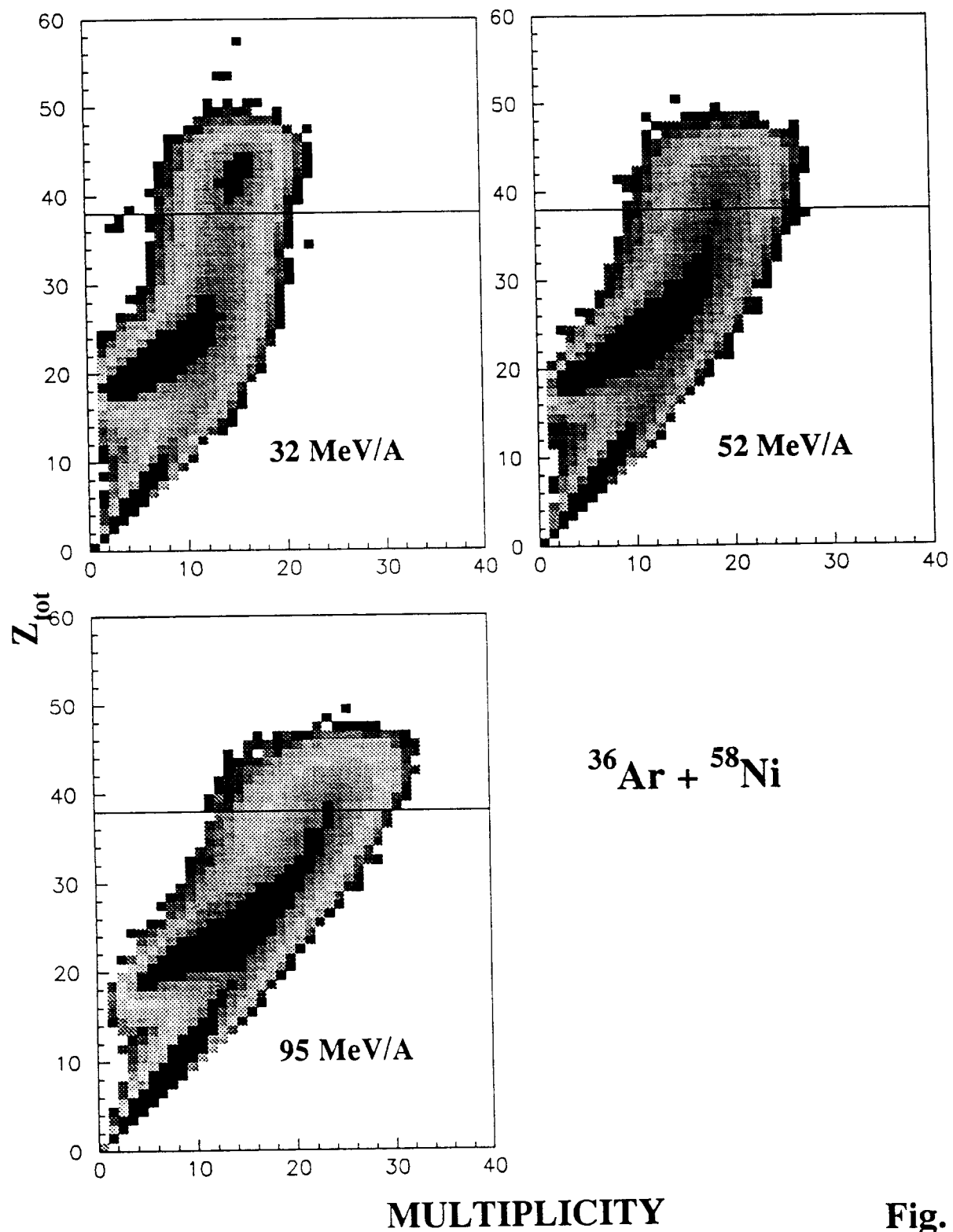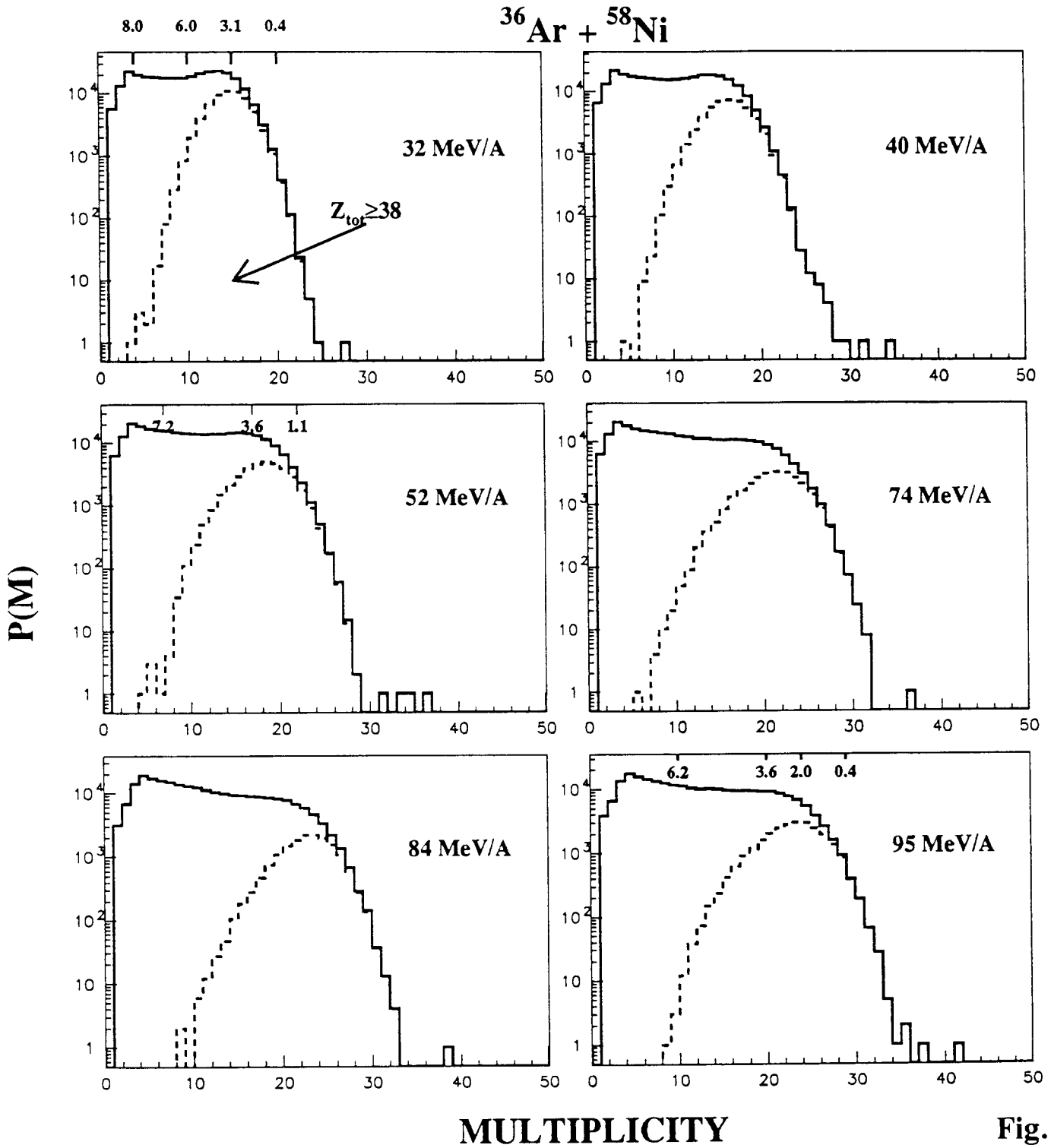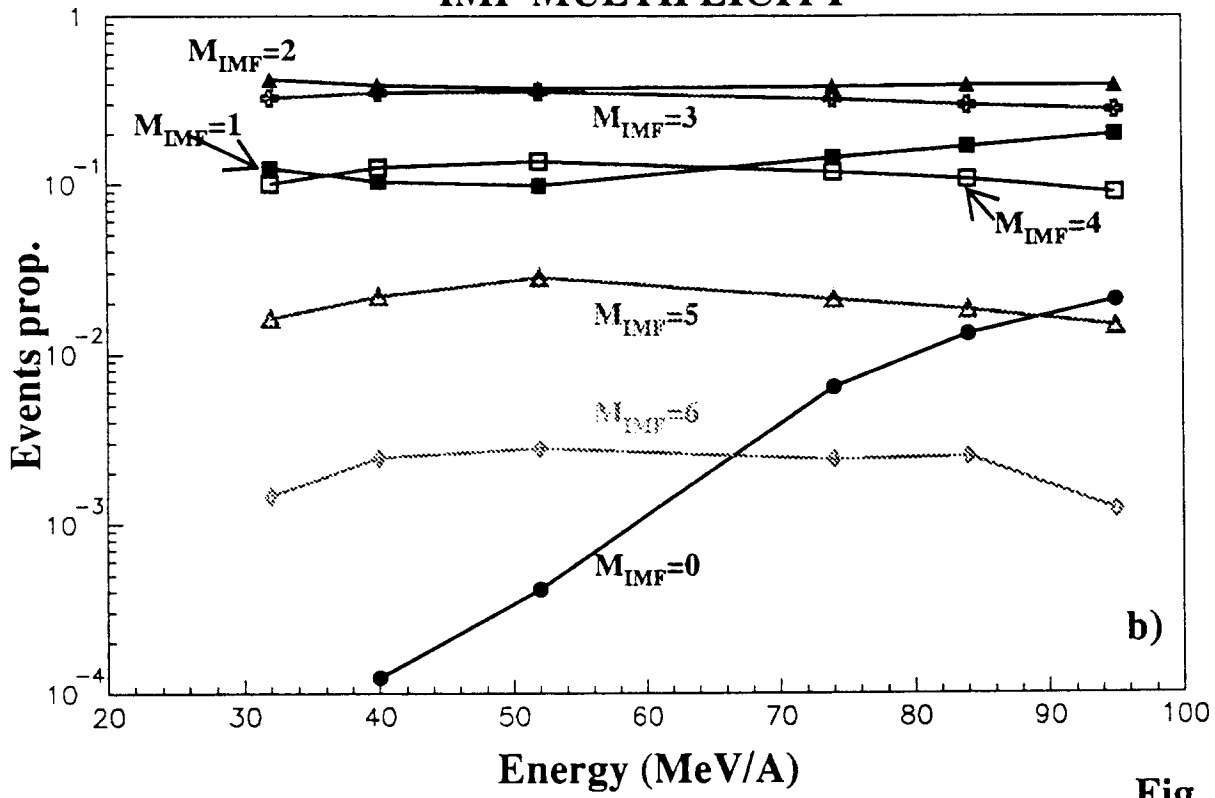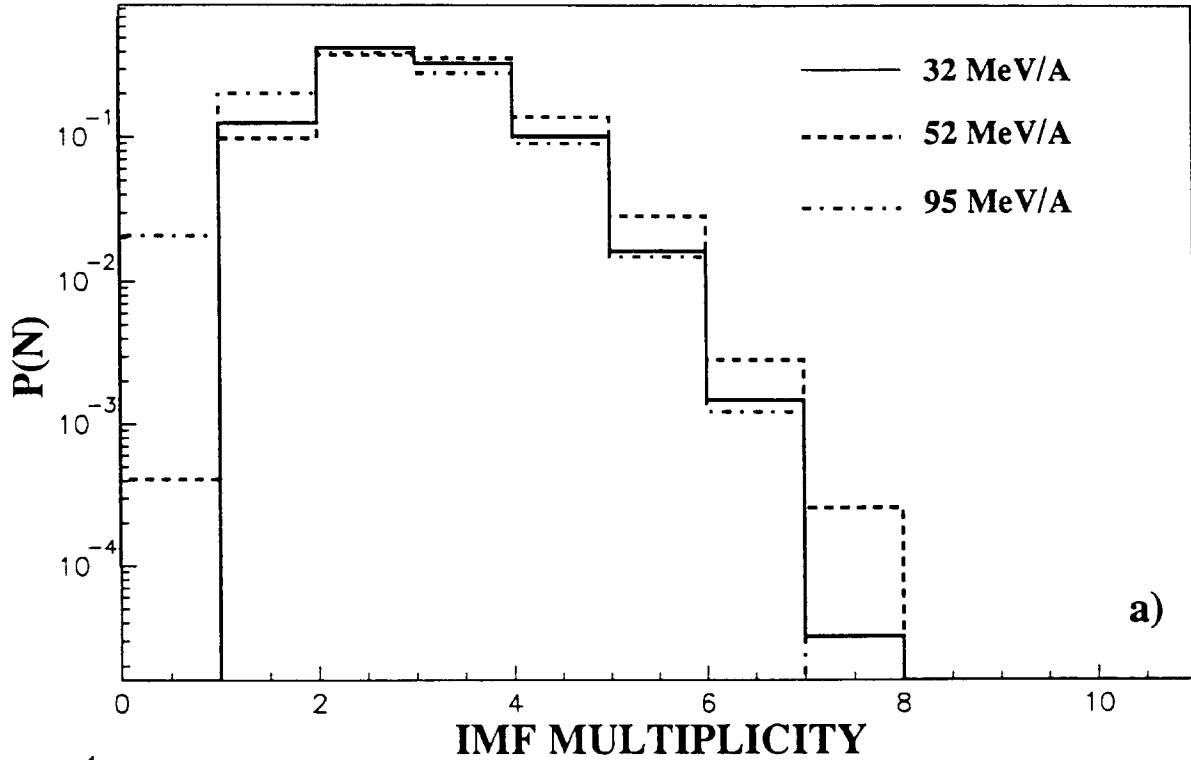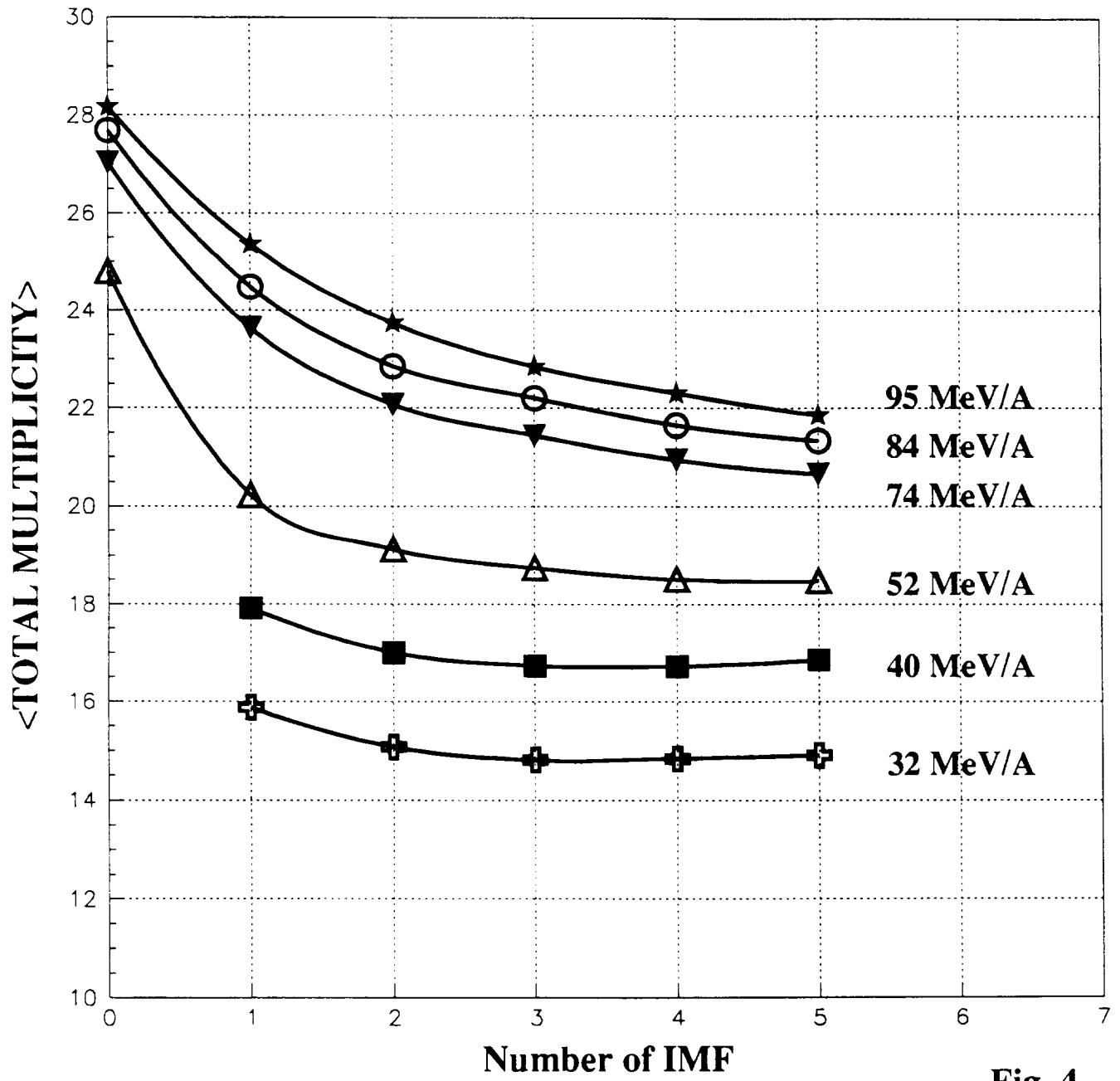
Fig. 4
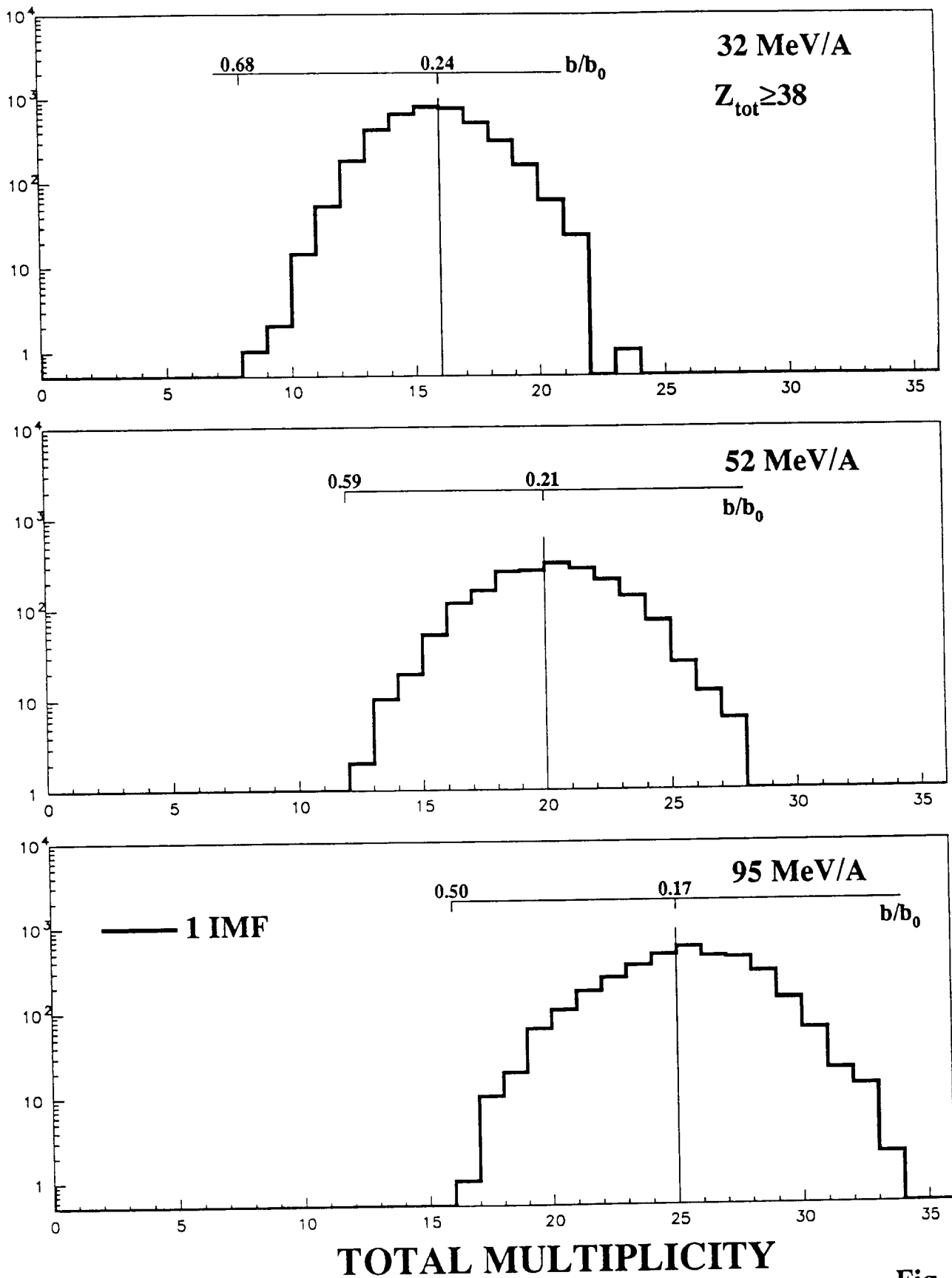
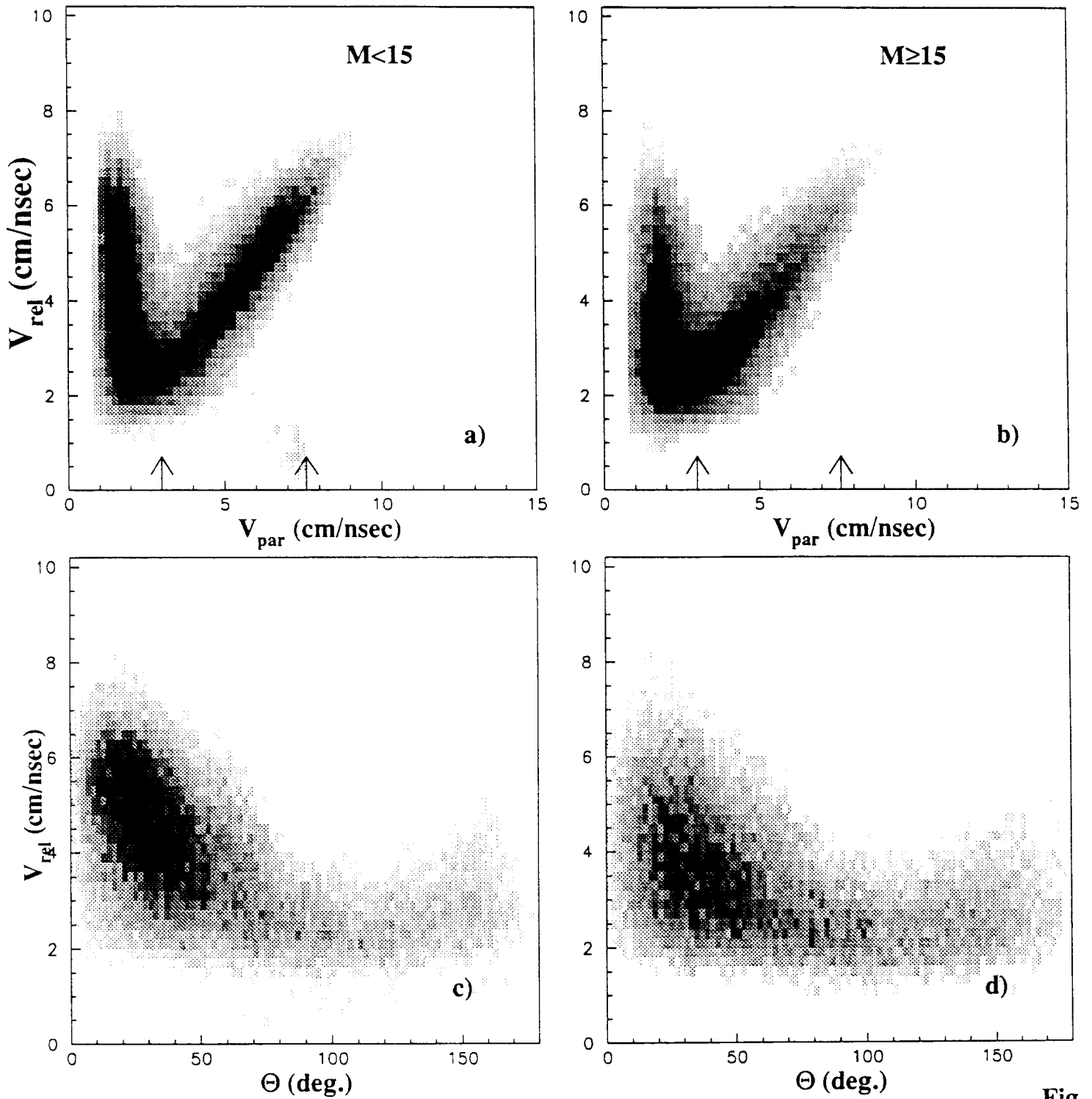Fig. 5
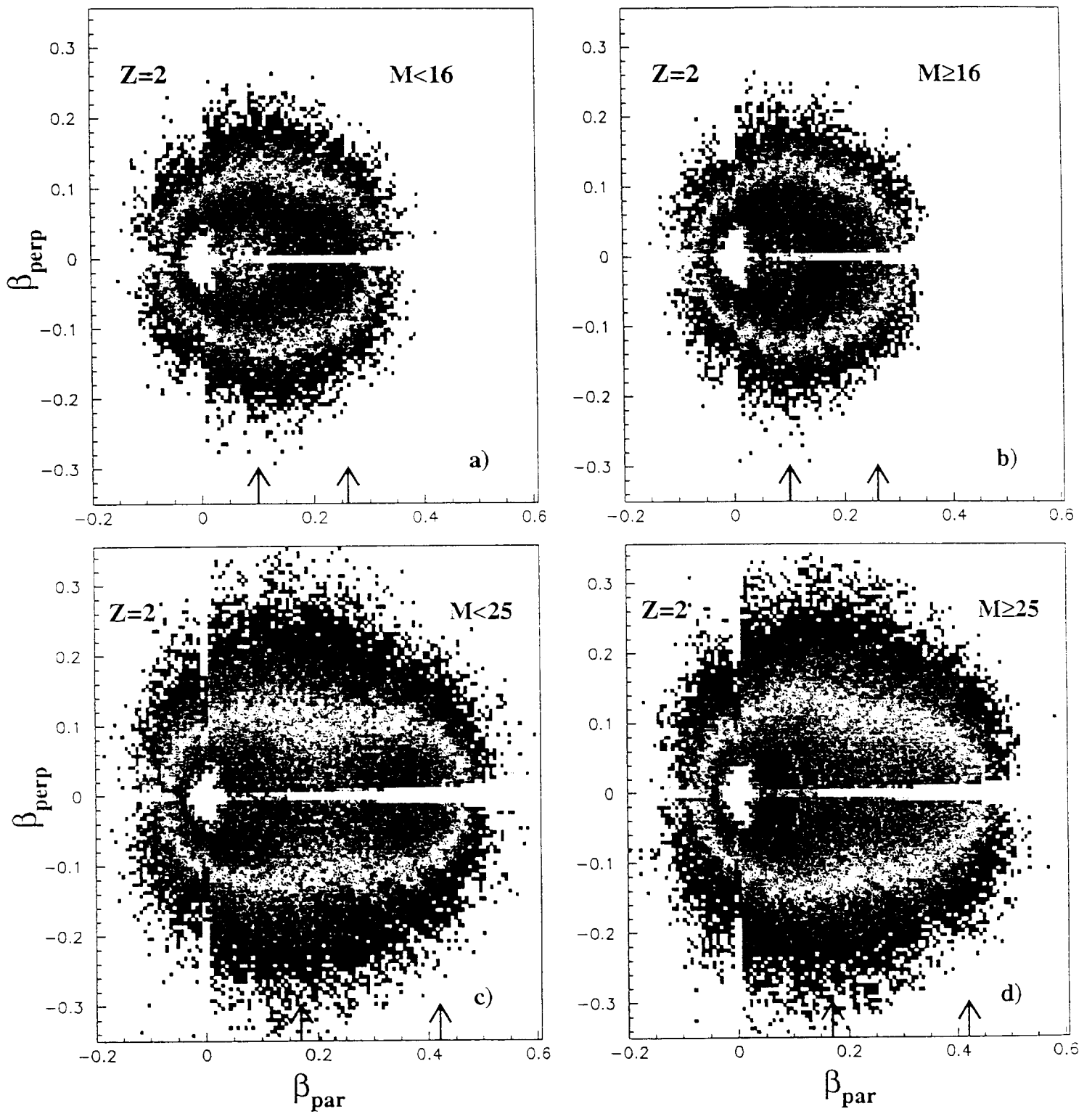
Fig. 6
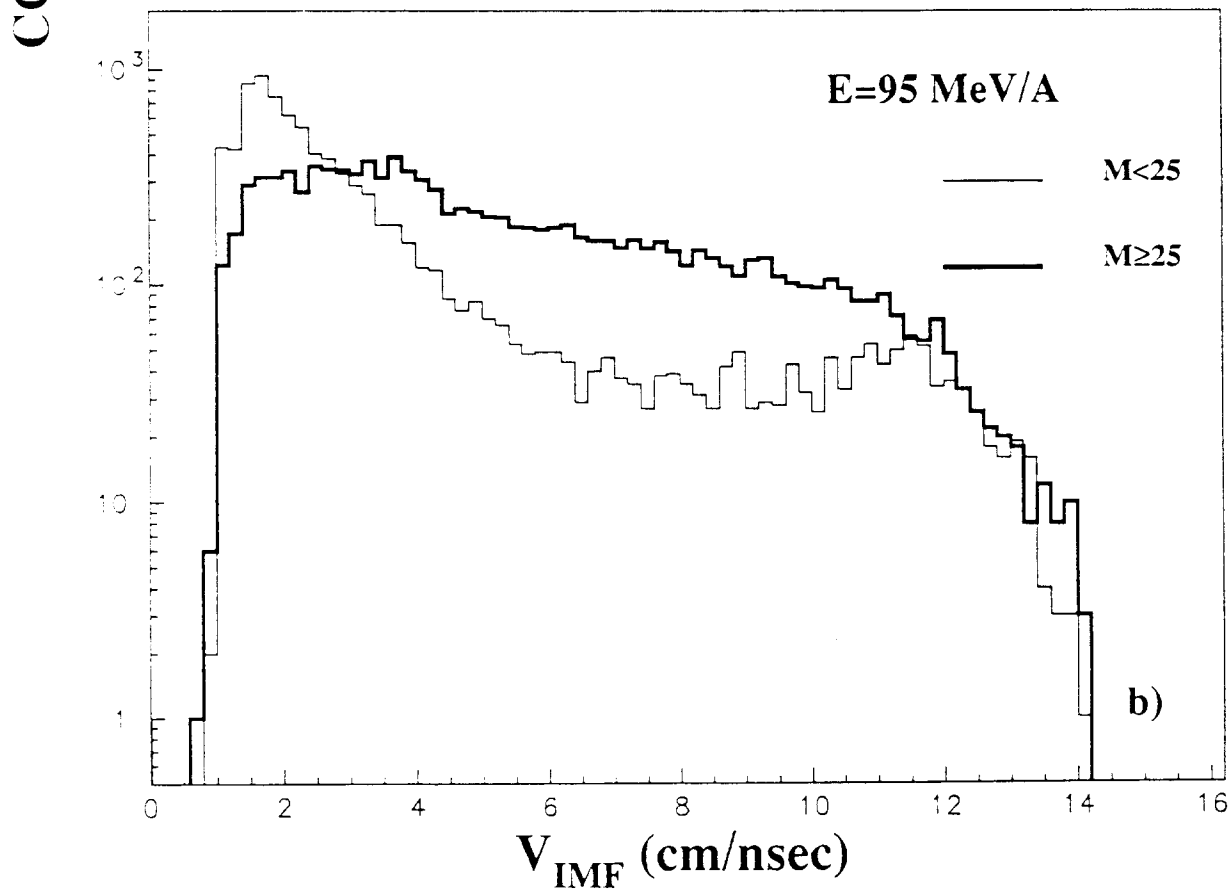
Fig. 7

Fig. 8

Ar + Ni 32 MeV/A (2 IMF $Z_{tot} \geq 38$)

Fig. 9

Ar + Ni 95 MeV/A

Fig. 10